Proceedings of the 11th Brazilian Congress of Thermal Sciences and Engineering -- ENCIT 2006
Braz. Soc. of Mechanical Sciences and Engineering -- ABCM, Curitiba, Brazil,- Dec. 5-8, 2006

Paper CIT06-0535

PREDICTION OF FLOW FIELD IN A CURVED CHANNEL

Yuu Itai
Grupo de Energia Bioamassa e Meio Ambiente-Departamento de Engenharia Mecânica- Universidade Federal do Pará, Belém-PA-Brasil, CEP:66075-110.
Yuu_itai@yahoo.com.br

Ricardo W. M. Ferreira
Departamento de Engenharia Mecânica- Universidade Federal do Pará, Belém-PA-Brasil, CEP:66075-110.
caco_bassa@yahoo.com.br

Danielle R.S. Guerra
Grupo de Energia Bioamassa e Meio Ambiente-Departamento de Engenharia Mecânica- Universidade Federal do Pará, Belém-PA-Brasil, CEP:66075-110
daguerra@ufpa.br

André L. A. Mesquita
Departamento de Engenharia Mecânica- Universidade Federal do Pará, Belém-PA-Brasil, CEP:66075-110
andream@ufpa.br

Abstract. *Flows with three dimensional effects are encountered in turbo machines and around complex bodies. These effects can be produced by channel with curved walls that provides curvature or change direction of the streamlines. The experimental study of the three-dimensionality and the structure of the turbulent flows, usually require optical techniques like the laser-Doppler anemometry or the particle image velocimetry systems, PIV. However, high costs of the experimental apparatus associated with these methods make these techniques inaccessible to many. Turbulent flows with streamline curvature are of considerable engineering interest. The aim of this work is to present the three dimensional effects of the turbulent air flow in a curved channel through the commercial code FLUENT 6.0. Three turbulence models were applied to obtain the mean velocity field and pressure gradients. In this study the grid of the geometry was development from dimensions of the wind tunnel located at the Fluid Mechanics Laboratory – DEM/UFPA. The wind tunnel has a curved rectangular test section of 150x300mm, with a fully developed channel flow.*

Keywords*.curved channel, streamline, velocity profile.*

1. Introduction

Computational fluids dynamics codes used to simulate cases have had an important place among the methods analysis and structures construction. Although it is necessary the knowledge of what appropriate model had been used in our case. Is completely necessary the use of commercial codes because the expensive costs of optical equipment adopted to measure the three-dimensional effects and draining structure turbulent. These variables usually require the use of optic techniques as anemometry for Laser-Doppler or systems of attainment of the field of speed for particle image, PIV, and it is represent a problem when doesn't have a lot of investments becoming practically inaccessible to some laboratories.

Shao et al. (2002) developed a simulation model which uses Reynolds averages, 3D Navier Stokes equations based on a boundary-fitted orthogonal curvilinear coordinate system. Two approaches for equation system closure are used, i.e, algebric stress models and nonlinear k - ε model for eddy viscosity. The different closure approaches have been discussed and the model was validated using measurements in curved rectangular channels. Predicted turbulence and secondary flow patterns in curved compound channel were compared with straight channels measurements.

Kim et al. (1994) investigated the developing turbulent flow in a 90 deg curved duct of rectangular cross section, and an aspect radio of 6 was investigated. The mean-velocity was measured with a five-hole pressure probe and Reynolds-stress components was measured with two sensors hot-wire probes, in the boundary layers on the duct walls to document the pressure driven secondary motion and the formation of a longitudinal vortex near the corner in the convex wall.

Shima et al. (2000), tested a low-Reynolds-number second-moment closure without wall-reflection redistribution terms in wall-bounded turbulent flows with streamline curvature. The turbulence model was previously shown to give good predictions for a fully developed channel flow, adverse and favorable pressure gradients, plane and round jets, and flows with wall blowing and suction and other good predictions. The model is used to calculate two fully developed curved channel flows and four boundary layers on curved walls. The turbulence model captures main features of the stabilizing and destabilizing effects of streamline curvature, though some notable discrepancies between the predictions and measurements are present in boundary layers on convex walls.

Silva et al. (1998) has an objective and good explanation to turbulence phenomenon and their variants. Treaster et al. (1979) developed programs to calibrate and employ five-hole probes of both angle tube and prismatic geometries and discuss about the applications.

Iacovides et al. (1990) reported a computational and experimental study of turbulent flow around a square-sectioned U-bend. All velocities measurements were obtained with DISA and TSI constant-temperature, hot-wire anemometers using standard DANTEC single and cross-wire probes. The flow prediction was studied by a software including the turbulence model.

Humphrey et al (1981) investigated steady, incompressible, isothermal developing flow in a square-section curved (comprises a 90° perpex bend) duct with smooth walls. The measurements (the longitudinal and radial components of mean velocity and corresponding components of the Reynolds stress tensor) were obtained with a Laser Doppler anemometer. Calculated mean velocity results obtained from solution of elliptic differential equations in finite difference form and incorporating a two-equation turbulence model are not strongly dependent on the model.

Schlichting (1968) presents the explanation of sprouting, development and separation of boundary layer. With a different way these studies insert values to this work.

The documentation of commercial code FLUENT 6.0 (2005) explains very well the equations of transport and turbulent models. What the appropriated cases to apply the turbulence model and the restrictions and vantages of all the models.

The present paper compare three turbulence models inserted on the commercial code FLUENT 6.0 analyzing their performance during the air draining in a wind tunnel, located at the Fluid Mechanics Laboratory – DEM/UFPA. The wind tunnel has a curved rectangular test section of 150x300mm, with a fully developed channel flow.

2. Case Description

The mesh was created in the commercial code GAMBIT 2.0, that was developed to create geometry and meshes, where a boundary layer its developed to facilitate the calculations refining the places closer of the wall. The mesh was constructed with a growth factor of 0.005 and B/A tax of 1.055 to the part that contain the curvature and the rectangular part. The structure has been shared in three parts becoming easier to create the boundary layer and the mesh. Two rectangular parts were meshed with 0.025 of size on the HEX MAP mode and the curvature with 0.008 on the same mode of the rectangular parts.

Two zones were been defined, the entrance with velocity inlet and the exit with pressure outlet. We have to point out the way that the structure will be meshed. It is completely important when the calculation run to converge. The order of mesh command to elements also has been discussed since for each structure has a different way to apply and create the perfect mesh. The first volume presents 15400 elements and 17388 nodes, the second part, that represents the curve, had 179200 elements and 194292 nodes and the third part contains 18200 elements and 20412 nodes, totalizing 212800 elements and 230580 nodes. Figure 1 shows the structure of curvature presents at the wind tunnel located at the Fluid Mechanics Laboratory – DEM/ UFPA. At Fig. 2 it showed a structure of curvature detail and it seemed that the structure presents a uniform and good mesh.

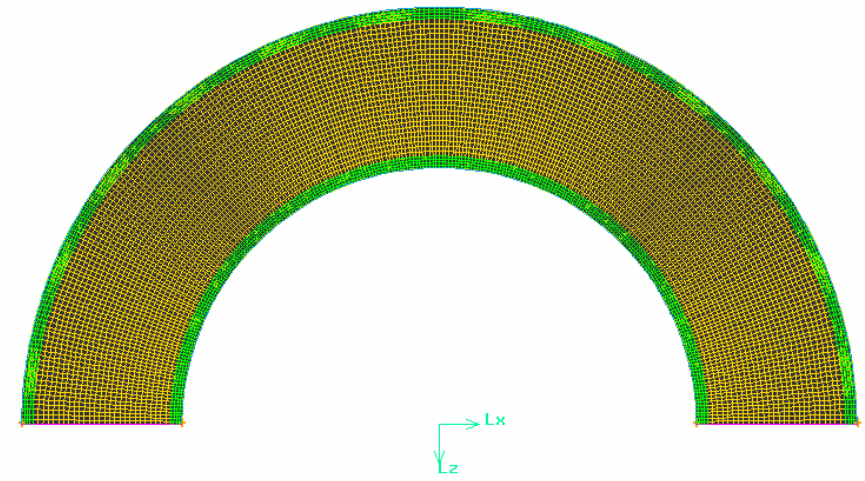

Figure 1 – The grid mesh of curvature of wind tunnel.

At Figure 3 it showed the two rectangular structures that united at the curvature showed at Figure 1 form the complete structure of wind tunnel. Figure 4 shows the grid detail of the mesh of rectangular parts that forms the wind tunnel.

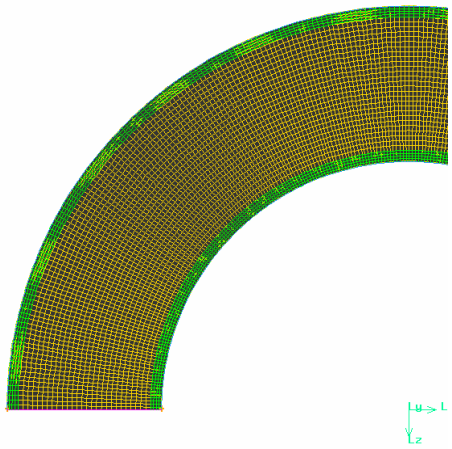

Figure 2 – A specific detail of mesh structure of curvature at wind tunnel.

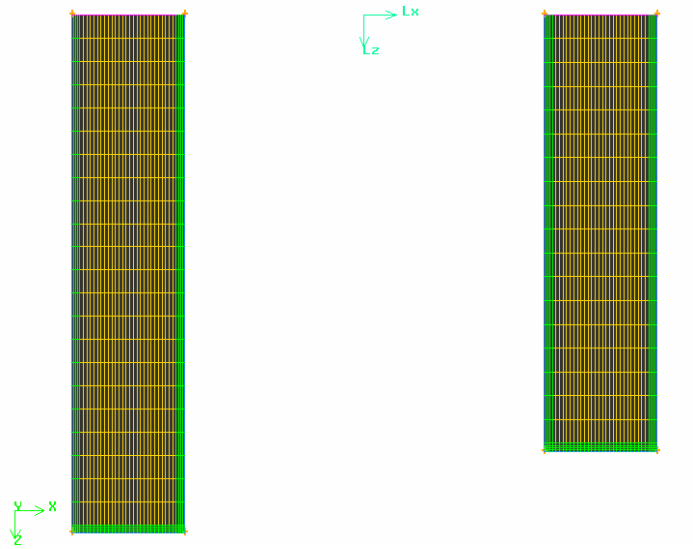

Figure 3 – Rectangular structures presents at the wind tunnel.

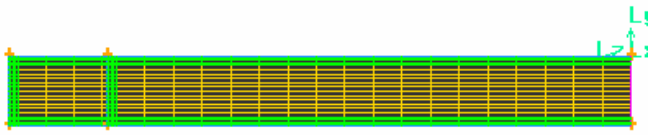

Figure 4 – Grid detail of rectangular structures of wind tunnel.

Figure 5 – The wind tunnel.

3. Turbulence Models

Three turbulence models have been chosen for the accomplishment of this work. The Standard *k* - ε the RNG *k* - ε and the Reynolds Stress Model (RSM). This explanation is based on FLUENT 6.0 Documentation (2005).

3.1. The Standard *k* - ε Model.

The Standard *k* - ε Model are very simple of "complete models" of turbulence are two-equation models in which the solution of two separate transport equations allows the turbulent velocity and length scales to be independently determined. Since it was proposed the standard *k* - ε model becomes the workhorse of practical engineering flow calculation. Robustness, economy, and reasonable accuracy for a wide range of turbulent flows explain the popularity in industrial flow and heat transfer simulations.

The standard *k* - ε model is a semi-empirical model based on model transport equations for the turbulence kinetic energy (*k*) and its dissipation rate (ε). The model transport equation for *k* is derived from the exact equation, while the model transport equation for ε was obtained using physical reasoning and bears little resemblance to its mathematically exact counterpart. In the derivation of the *k* - ε model, it was assumed that the flow is fully turbulent, and the effects of molecular viscosity are negligible. The standard *k* - ε model is therefore valid only for fully turbulent flows. The turbulence kinetic energy, *k*, and rate of dissipation, ε, are obtained from the following transport equations:

$$\frac{\partial}{\partial t}(\rho k)+\frac{\partial}{\partial x_i}(\rho k u_i)=\frac{\partial}{\partial x_j}\left[\left(\mu+\frac{\mu_t}{\sigma_k}\right)\frac{\partial k}{\partial x_j}\right]+G_k+G_b-\rho\varepsilon-Y_M+S_k \qquad (3.1.1)$$

and

$$\frac{\partial}{\partial t}(\rho \varepsilon)+\frac{\partial}{\partial x_i}(\rho \varepsilon u_i)=\frac{\partial}{\partial x_j}\left[\left(\mu+\frac{\mu_t}{\sigma_\varepsilon}\right)\frac{\partial \varepsilon}{\partial x_j}\right]+C_{1\varepsilon}\frac{\varepsilon}{k}(G_k+C_{3\varepsilon}G_b)-C_{2\varepsilon}\rho\frac{\varepsilon^2}{k}+S_\varepsilon \qquad (3.1.2)$$

In these equations, G_k represents the generation of turbulence kinetic energy due to the mean velocity gradients, G_b is the generation of turbulence kinetic energy due to buoyancy, Y_M represents the contribution of the fluctuating dilatation in compressible turbulence to the overall dissipation rate. $C_{1\varepsilon}$, $C_{2\varepsilon}$, and $C_{3\varepsilon}$ are constants. σ_k and σ_ε are the turbulent Prandtl numbers for *k* and ε, respectively. S_k and S_ε are user-defined source terms. The turbulent (or eddy) viscosity, μ_t, is computed by combining *k* and ε as follows:

$$\mu_t=\rho C_\mu\frac{k^2}{\varepsilon} \qquad (3.1.3)$$

Where C_μ is a constant.

The model constants $C_{1\varepsilon}$, $C_{2\varepsilon}$, C_μ, σ_k and σ_ε have the following default values :

$$C_{1\varepsilon}=1.44,\ C_{2\varepsilon}=1.92,\ C_\mu=0.09,\ \sigma_k=1.0,\ \sigma_\varepsilon=1.3 \qquad (3.1.4)$$

These default values have been determined from experiments with air and water for fundamental turbulent shear flows including homogeneous shear flows and decaying isotropic grid turbulence. They have been found to work fairly well for a wide range of wall-bounded and free shear flows.

3.2. The RNG *k* - ε Model.

The RNG *k* - ε model was derived using a rigorous statistical technique (called renormalization group theory). It is similar in form to the standard *k* - ε model, but includes the following refinements: The RNG model has an additional term in its equation that significantly improves the accuracy for rapidly strained flows, the effect of swirl on turbulence is included in the RNG model, enhancing accuracy for swirling flows. On RNG theory provides an analytical formula for turbulent Prandtl numbers, while the standard *k* - ε model uses user-specified, constant values. While the standard *k* – ε model is a high-Reynolds-number model, the RNG theory provides an analytically-derived differential formula for

effective viscosity that accounts for low-Reynolds-number effects. Effective use of this feature does, however, depend on an appropriate treatment of the near-wall region.

These features make this model more accurate and reliable for a wider class of flows than the standard k - ε model. This model is derived from the instantaneous Navier-Stokes equations. The analytical derivation results in a model with constants different from those in the standard k - ε model, and additional terms and functions in the transport equations for k and ε.

3.2. The Reynolds Stress Model.

The Reynolds stress model (RSM) is the most elaborate turbulence model that the commercial code FLUENT 6.0 provides. Abandoning the hypothesis of isotropic eddy-viscosity, the RSM closes the Reynolds-averaged Navier-Stokes equations by solving transport equations for the Reynolds stresses, together with an equation for the dissipation rate. This means that five additional transport equations are required in 2D flows and seven additional transport equations must be solved in 3D.

Since the RSM accounts for the effects of streamline curvature, swirl, rotation, and rapid changes in strain rate in a more rigorous manner than one-equation and two-equation models, it has greater potential to give accurate predictions for complex flows. However, the fidelity of RSM predictions is still limited by the closure assumptions employed to model various terms in the exact transport equations for the Reynolds stresses. The modeling of the pressure-strain and dissipation-rate terms is particularly challenging, and often considered to be responsible for compromising the accuracy of RSM predictions.

The RSM might not always yield results that are clearly superior to the simpler models in all classes of flows to warrant the additional computational expense. However, use the RSM is a must when the flow features of interest are the result of anisotropy in the Reynolds stresses. Among the examples are cyclone flows, highly swirling flows in combustors, rotating flow passages, and the stress-induced secondary flows in ducts.

4. Results

The simulation was conducted considered that the initial velocity was 10 m/s and the outlet pressure was 101325 Pa. Using the turbulence models we compared results of velocity and pressure gradients. All the models have a good convergence. Although some models results are greater than others and lately we discuss the results. We have to create six planes to show better the velocity behavior along the wind tunnel. The Fig. 6 shows where the planes are located.

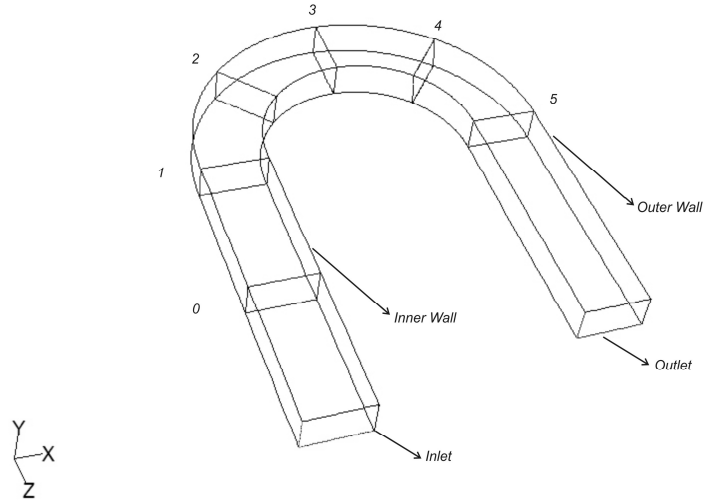

Figure 6 – The six planes created in wind tunnel with a strong curvature.

Figure 7 shows the profiles of the longitudinal velocity component, U, across de duct, from the outer to the inner wall at the six planes. The corresponding distributions of the V and W components are not shown. At plane 0, the velocity profile shows a flat plate type boundary layer. Plane 1 is the position where the curved section begins, at this plane the longitudinal velocity increase near the inner wall.

At plane 2 the longitudinal velocity increases more close to the inner wall and decrease until the outer wall. These effects are repeated in the middle of the curvature at plane 3. However, at the plane 3 the longitudinal velocity near the inner wall begins to decrease.

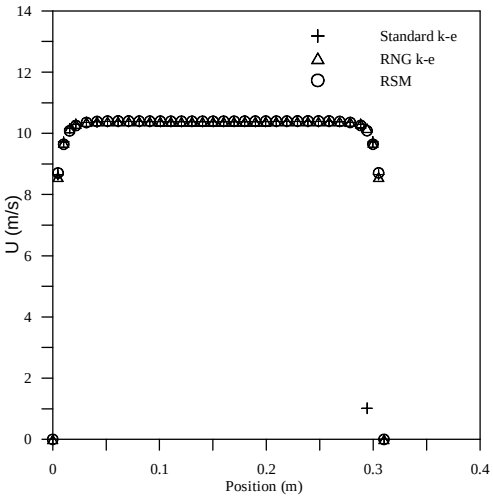

(a) Plane 0, at the middle of the first straight section.

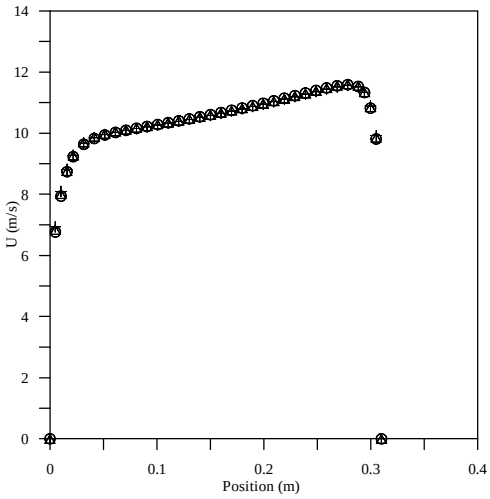

(b) Plane 1, upstream of the bend.

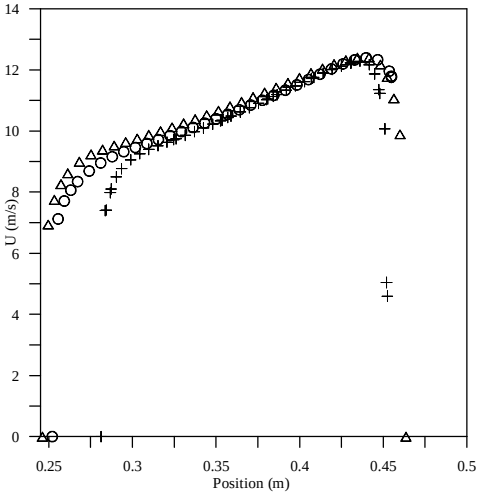

(c) Plane 2, at the first curvature.

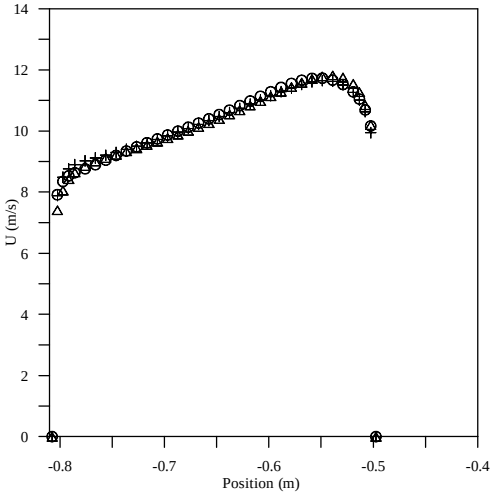

(d) Plane 3, at the middle of the curvature.

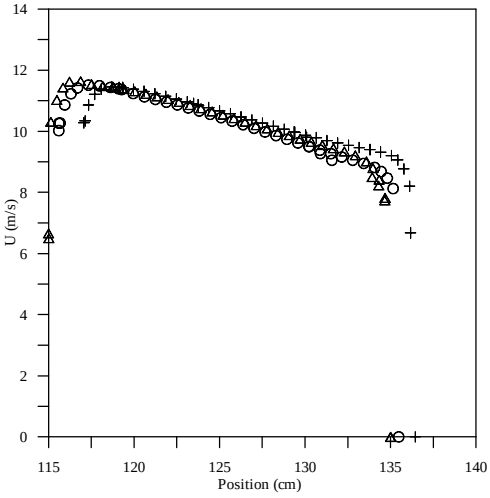

(e) Plane 4, at the second curvature.

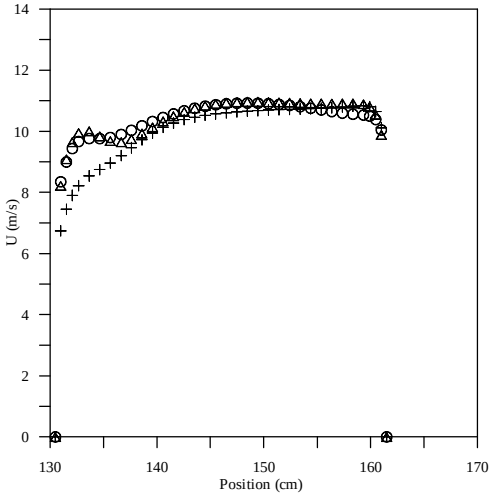

(f) Plane 5, at the exit of bend.

Figure 7 – Longitudinal velocity predicted by the three turbulent models, from outer to inner wall: (a) at plane 0, (b) at plane 1, (c) at plane 2, (d) at plane 3, (e) at plane 4 and (f) at plane 5.

At plane 4, the effect is changed, the longitudinal velocity is increased near the outer wall and presents diminish close to the inner wall. Finally, at plane 5 we can note the presence of a longitudinal vortex through the profiles of U, which depict the two peaks commonly observed in flows with vortex. These observations are consistent with the effect of concave curvature which acts to increase turbulent mixing and leads to increase velocity close to the wall.

It was observed that the pressure distribution along the channel walls is strong determined by the curvature. The pressure gradients induced by the curvature are clearly seen. The results of simulation indicated that on the inner wall, the boundary layer is subjected to a favorable pressure gradient starting upstream of the bend, close to the plane 1, where is found the higher velocities.

According Kim et al (1994) the transition of the flow of the curve for the straight line causes a reduction of the pressure in the concavous wall and increase in the convex wall, generating in this last adverse gradient of pressure, propitious condition to the separation of the boundary layer.

The results for longitudinal velocity profiles predicted by the three turbulent models have shown the same behavior for all planes. At the inlet, plane 0, and upstream the bend, plane 1, all three turbulence models predicted very well the longitudinal velocity. The Standard k - ε model provided poor results for the velocity near the wall when the flow presents a strong curvature, it can be observed in the Figures 7(c) and 7(e), planes 2 and 4. At the exit of the bend, this turbulence model was not able to predict the effect of the longitudinal vortex as shown in the Figure 7(f).

The other two turbulence models, RNG $k - \varepsilon$ and Reynolds stress model, have predicted longitudinal velocity data more close to the wall than the Standard k - ε model. These two models were able to capture the presence effect of a longitudinal vortex. This effect can be seen by the peak on the longitudinal profile in Figure 7(f).

The results below are the bidimensional planes, (x, y), at the planes 0, 1, 2, 3, 4 and 5. Figure 8 (a, b, c, d, e and f), Figure 9 (a, b, c and d) and Figure 10 (a, b, c and d) shown the predicted secondary flow using the three turbulence models described above. The Figures are shown in velocity vectors colored by velocity magnitude (m/s).

In a curved duct of rectangular section it was noticed the secondary flows of first and second type, determined respectively for the bending and the rectangular form of the section.

The results in Figure 8(a) and (b) have shown that in the straight section there was not secondary flow. The same behaviour was seen in the vectors provided by the simulation using the RNG $k - \varepsilon$ and the RSM models, at planes 0, 1 and 3.

At plane 2 in the first curvature, the Standard $k - \varepsilon$ indicated strong inclined currents; this region presents two vortex, one at the right side close to the inner wall, one at the top of the outer wall. At this plane is clearly seen the region of higher velocities. Again, at plane 4, in the second curvature, it can be seen inclined secondary currents; no vortex was predicted by the Standard $k - \varepsilon$ in this region.

Humphrey et al. (1981) considered that the secondary flows of first type is created from the disequilibrium between the centrifugal force and the gradient of radial pressure acting on the fluid of the boundary layer of the sidewalls of the curve, changing it, throughout these walls, for the internal region of the curve. The continuity demands a corresponding movement dislocating fluid, throughout the plan of symmetry, of the convex wall (internal region) for concaves wall (external) of the curve, generating itself thus the two great vortices in against rotation characteristic of the draining in curved duct. And this type of secondary flow can be seen in the Plane 2 and 4.

At plane 5, the model predicted an asymmetric secondary flow. In this region the higher velocities are concentrated close to the outer wall. Schlichting (1968) explain that the secondary flows of second type occur throughout the bisector in direction to the corner, where it bifurcate and it returns in opposing directions. This second type of secondary flows is weak than the first type and it's seemed for the elongation of isolines of velocity in direction to the corner. And this type can be seen at the Planes 3 and 5.

Iacovides et al (1990) explain the secondary motion in modifying the streamwise flow. This flow is deflected down the inside wall toward the duct mid-plane and a return flow occurs from the inside to the outside over the core region of the duct.

This is the classical single-cell vortex flow that pertains at the 45-degree station. By 90 deg, the readjustments to the streamwise velocity field lead, through its coupling with the pressure fields, to the eye of the secondary vortex being pushed far to the inside to the bend. This is what causes the development of “mushroom” shaped velocity contours near the inner wall as the return fluid is deflected away from the center plane; indded, it is displacement of low-momentum fluid near the center plane that is directly responsible for the “troughs”. And it can be seen at the Fig. 7 (f), 8 (f), 9 (c) and 10(c).

Figure 9 shows the results provided by the RNG $k - \varepsilon$. These predictions were different from the predictions provided by the Standard $k - \varepsilon$. Plane 2 presents strong inclined secondary currents that forms two vortex at the opposite position of that predicted by the Standard $k - \varepsilon$.

At Plane 4 appears a vortex close to the outer wall. The same behaviour predicted by the Standard $k - \varepsilon$ for the pane 5 can be seen again. However, the RNG $k - \varepsilon$ can capture the strong curvature of the streamlines and predicted the growth of two vortex close to the inner wall.

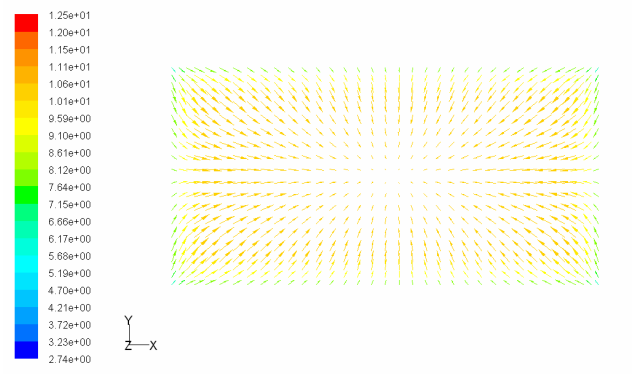

(a) Plane 0, at the middle of the first straight section.

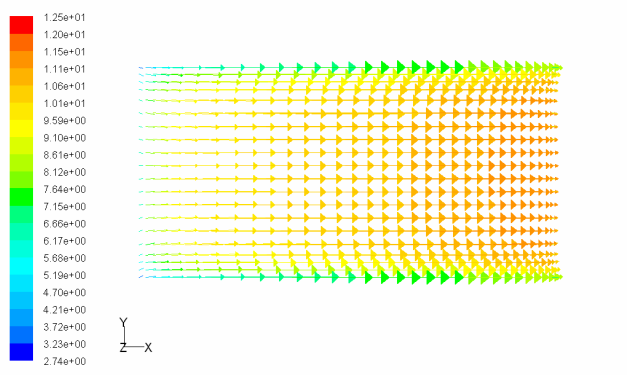

(b) Plane 1, upstream of the bend.

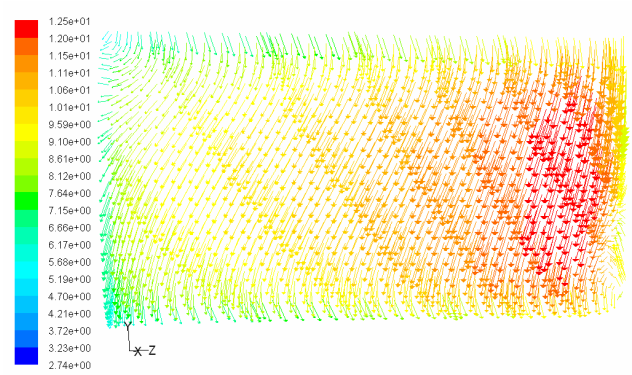

(c) Plane 2, at the first curvature.

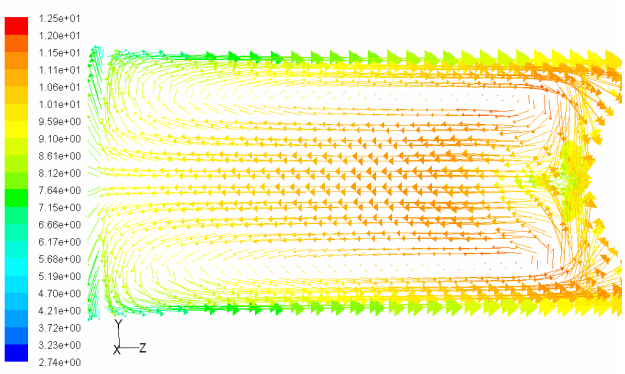

(d) Plane 3, at the middle of the curvature.

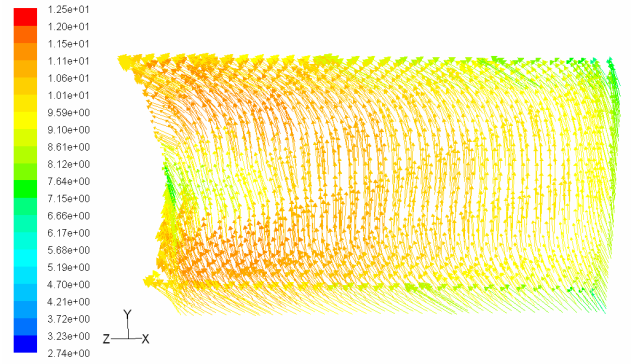

(e) Plane 4, at the second curvature.

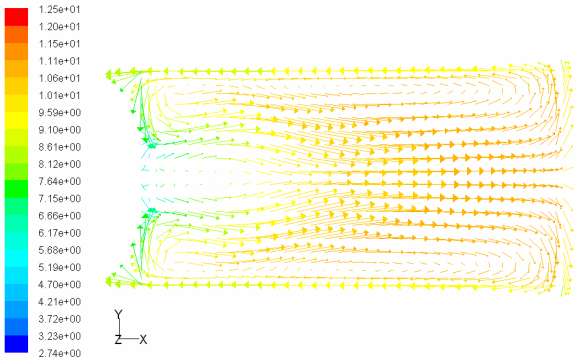

(f) Plane 5, at the exit of bend.

Figure 8 – Secondary flow predicted by the Standard k - ε model, from outer to inner wall: (a) at plane 0, (b) at plane 1, (c) at plane 2, (d) at plane 3, (e) at plane 4 and (f) at plane 5.

Results of the RSM are shown in Figure 10. It can be seen a similar behavior to that have founded by the others turbulence models. However, there was not an agreement on the prediction of the vortex that appears at plane 2. This model can not able to predicted a vortex near the outer wall at plane 4 as seen by the results of RNG k – ε.

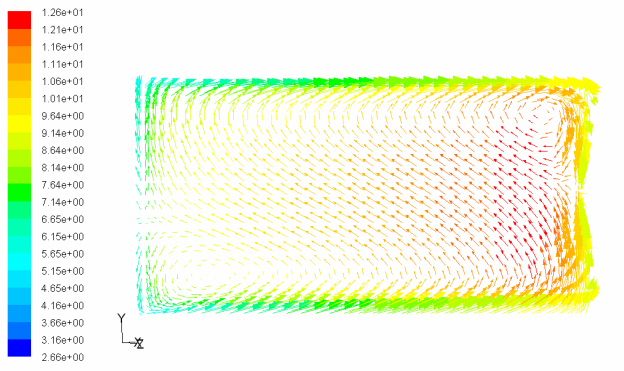

(a) Plane 2, at the first curvature.

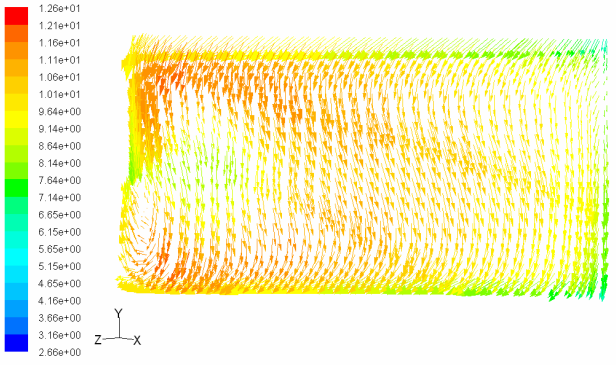

(b) Plane 4, at the second curvature.

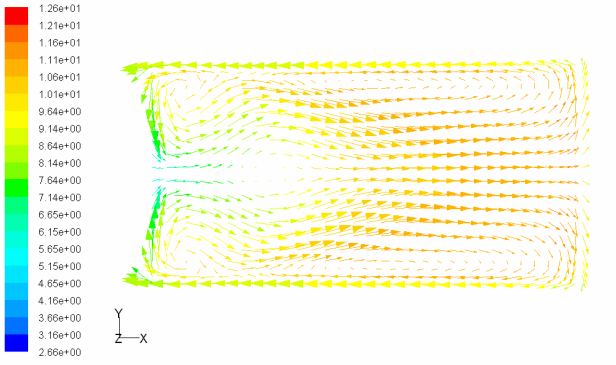

(c) Plane 5, at the exit of bend.

Figure 9 – Secondary flow predicted by the RNG k – ε model: (a) at plane 2, (b) at plane 4 and (c) at plane 5.

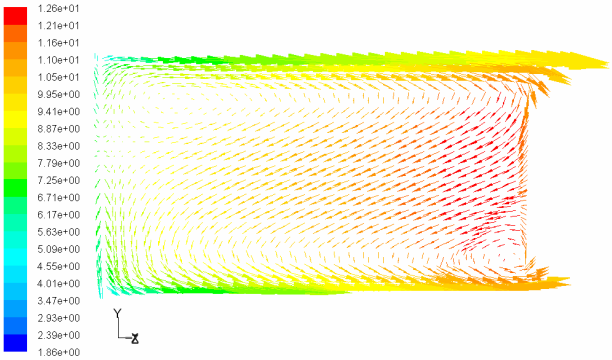

(a) Plane 2, at the first curvature.

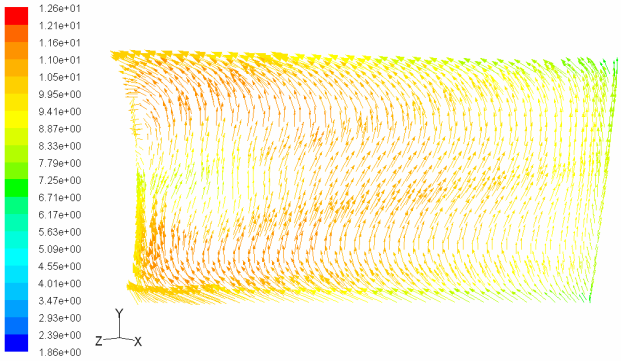

(b) Plane 4, at the second curvature.

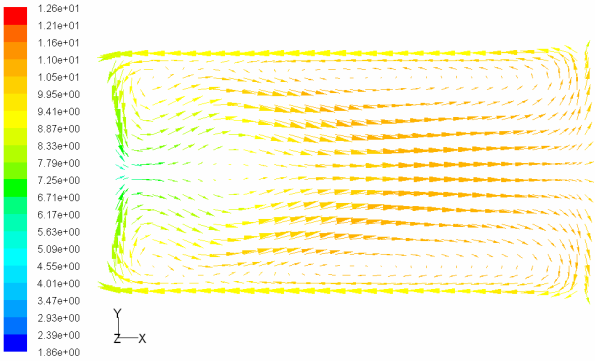

(c) Plane 5, at the exit of bend.

Figure 10 – Secondary flow predicted by the RSM: (a) at plane 2, (b) at plane 4, (c) at plane 5.

3. Conclusion

Three turbulence models were tested successfully to the prediction of the longitudinal velocity and secondary flow in a curved test section of a wind tunnel. The RNG $k - \varepsilon$ model has provided better results. This model has indicated the best profile of velocity magnitude at the exit of wind tunnel and has shown the best contour of velocity magnitude. But the profiles of the Standard $k - \varepsilon$ and the RSM model were not bad.

The RNG $k - \varepsilon$ model improves the accuracy for rapidly strained and swirling flows. This characteristic of the model appears on the results of the prediction of the secondary flow. The good results provided by the RSM model is due it is more complete than the others two models because have more equations and has the greater potential to give accurate predictions for complex flows.

The wind tunnel flow is little complex because the constant values of velocity develop a profile that changes a lot during the simulation. At first is constant, in a second time is concentrated at the internal part of curvature and finally changes to opposite side and finish with developed flow.

To the static pressure the profile obtained are similar to three turbulence models. At first time it constant in the curvature, developed a higher value at external part of curvature and at the finish is constant, but with a lesser value than the beginning. It is clearly that this behavior is a consequence of the curved channel.

The aim of this work was to provide the behavior of the flow that occurs in a wind tunnel located at the Fluid Mechanics Laboratory – DEM/ UFPA. Further effects, especially experimental validation are needed to improve the capability of the models for predicting flow with complex boundary conditions.

4. Acknowledgement

To the Energy Biomass and Environment Group – DEM/ UFPA that made possible the execution of this work.

5. References

Cheng, K.C., Yuen, F.P., 1987, “Flow visualization studies on secondary flow patterns in straight tubes downstream of a 180º bend and in isothermally heated horizontal tubes”, Trans. ASME, J. Heat Transfer, Vol.109, pp.49-61.

Humphrey, J. A. C., Whitelaw, J. H. and Yee, G., 1981, "Turbulent flow in a square duct with strong curvature", Journal of Fluid Mechanics, vol. 103 , pp. 443-463.

Iacovides, H., Lauber, B.E., Loizou P.A., Zhao, H.H., 1990, “Turbulent boundary-layer development around a square-sectioned U-bend: Measurements and computation.” ASME, Journal of Fluids Engineering, Vol.112, pp. 409-415.

Kim W.J., Patel V.C., 1994, “Origin and decay of longitudinal vortices in developing flow in a cuved rectangular duct”, Journal of Fluids Engineering, Vol.116, pp.45-52.

Shao X., Wang H., Chen Z., 2003, “Numerical modeling of turbulent flow in curved channels of compound cross section”, Advances in Water Resourses, Vol.26, pp.525-539.

Schlichting, H., 1968, "Boundary-Layer Theory", McGraw-Hill, New York.

Shima N., Kawai T., Okamoto M., Tsuchikura R., 2000, “Prediction of streamline curvature effects on wall-bounded turbulent flows”, International Journal of Heat and Fluid Flow, Vol.21, pp.614-619.

Silva, A.P.S., Menut P. P. P., Su J., 1998, “Turbulência”, Anais da I Escola de Primavera de Transição e Turbulência.

Treaster, A.L., Yocum, A.M., 1979, “The calibration and application of five-hole probes”, ISA Transactions, Vol.18, pp.23-34.

Yamamoto, K., Wu, Xiaoyun, Nozaki, K., Hayamizu, Y., 2006, “Visualization of Taylor-Dean flow in a curved duct of square cross-section”, Fluid Dynamics Research, Vol.38, pp.1-18.

Winters, K.H., 1987, “A bifurcation study of laminar flow in a curved tube of rectangular cross-section”, Journal Fluid Mechanics, Vol.180, pp. 343-369.

6. Copyright Notice